Materials Today Bio 29 (2024) 101312

Contents lists available at ScienceDirect

Materials Today Bio

journal homepage: www.journals.elsevier.com/materials-today-bio

Biodegradable exosome-engineered hydrogels for the prevention of peritoneal adhesions via anti-oxidation and anti-inflammation

Weitong Wang [a], Yuchen Ren [a], Qingyu Yu [b], Lijie Jiang [a], Chaojie Yu [b], Zhiwei Yue [a], Yue Wang [a], Jiajun Lu [a], Pengcheng Che [c,**], Junjie Li [b,***], Hong Sun [a,*]

[a] Department of Basic Medical Sciences, North China University of Science and Technology, Tangshan, 063210, China
[b] Frontiers Science Center for Synthetic Biology and Key Laboratory of Systems Bioengineering, Ministry of Education, School of Chemical Engineering and Technology, Tianjin University, Tianjin, 300350, China
[c] School of Nursing and Rehabilitation, North China University of Science and Technology, Tangshan, 063210, China

ARTICLE INFO

Keywords:
Peritoneal adhesions
Exosomes
Hydrogels
Immunoregulation

ABSTRACT

Peritoneal adhesions (PA) are a common and severe complication after abdominal surgery, impacting millions of patients worldwide. The use of anti-adhesion materials as physical barriers is an effective strategy to prevent postoperative adhesions. However, the local inflammatory microenvironment exerts a significant impact on the efficacy of anti-adhesion therapies. In this study, an injectable hydrogel based on oxidized dextran/carboxymethyl chitosan (DCC) is designed and prepared. Furthermore, the DCC hydrogel is specifically engineered to load the adipose mesenchymal stem cells (ADSCs)-derived exosomes (Exos) for the treatment of PA. The prepared DCC hydrogel can act as the physical barrier via covering the irregular wound surface effectively. Moreover, it shows controlled degradation property, enabling the regulated release of Exos. The DCC hydrogel loaded Exos (DCC/Exo) system has high antioxidant capacity, and can effectively modulate the inflammatory microenvironments and diminish apoptosis. Notably, it promotes a polarization shift towards the M2-like phenotype in macrophages. The RNA-seq analysis confirms that the DCC/Exo system exhibits significant anti-inflammatory properties and promotes a reduction in collagen deposition. Consequently, the DCC/Exo system can inhibit peritoneal adhesions significantly in a mouse cecum-abdominal wall injury model. These results demonstrate the DCC/Exo is an ideal material for preventing postoperative adhesions.

1. Introduction

Peritoneal adhesions (PA), a common and severe complication after abdominal surgery [1], result in the random development of vascularized and innervated fibrous connections involving the intestinal collaterals, peritoneum, and abdominal wall. Severe adhesions can cause abdominal pain, intestinal blockage and female infertility, thereby significantly impairing the quality of patients' postoperative lives and exacerbating psychological and economic burdens [2]. Previous study suggested that a significant proportion of patients (up to 79 %) who undergo abdominal or pelvic surgery may develop adhesions to varying degrees [3]. The formation of abdominal adhesions is influenced by a complex interplay of pathological factors, including tissue ischemia, hypoxia, oxidative stress, inflammation and excessive collagen deposition. Consequently, PA can significantly affect patient outcomes, underscoring the prevention of PA is a substantial challenge in clinical practice.

Improvements in surgical techniques, alongside pharmacological interventions and the use of physical barriers, constitute the main strategies for the prevention of postoperative abdominal adhesions [4,5]. Laparoscopy is a minimally invasive surgical technique used in clinical practice; however, it has been found to be insufficient in preventing PA [6]. Due to the limitations of drug therapy, such as suboptimal pharmacokinetics and possible side effects, physical barriers have increasingly become a focal point for preventing PA [7,8]. These Physical barriers can isolate the injured tissue directly and represent a common clinical method for postoperative adhesions prevention, including the use of solutions, films, and hydrogels. Among them, hydrogels are

* Corresponding author.
** Corresponding author.
*** Corresponding author.
E-mail addresses: chepengcheng@ncst.edu.cn (P. Che), li41308@tju.edu.cn (J. Li), sunhong@ncst.edu.cn (H. Sun).

https://doi.org/10.1016/j.mtbio.2024.101312
Received 23 April 2024; Received in revised form 16 August 2024; Accepted 24 October 2024
Available online 24 October 2024

promising materials for adhesions prevention, boasting a range of excellent properties such as superior exceptional biodegradability and versatile engineering flexibility. Notably, some hydrogels have been regulatorily approved for the clinical management of PA (*e.g.*, sodium hyaluronate). However, the design of these materials did not adequately incorporate the microenvironmental characteristics associated with adhesion formation. This oversight has resulted in inadequate prevention of inflammation and fibrosis [9]. Therefore, there is an imperative and urgent need for the development of physical barriers with microenvironment regulation function to achieve restorative effects.

Recent studies have emphasized the important role of stem cells in facilitating tissue repair and reducing scar formation. This is attributed to their capacity to suppress inflammation and prevent the excessive deposition of collagen [10–14]. Yang et al. found that adipose mesenchymal stem cells (ADSCs) promote peritoneal regeneration and facilitate tissue repair effectively by modulating macrophage polarization. This property renders ADSCs a favorable option for wound healing and tissue regeneration applications [15–18]. However, the stem cell therapy faces several challenges, including the cell viability, potential immunogenicity, and the risks associated with tumorigenesis [19]. A previous study revealed that ADSCs mainly exert their effects through the secretion of exosomes (Exos) [20]. These ADSCs-derived Exos exhibit similar biological functions with ADSCs but possess the advantages of less immunogenic and more stable. Moreover, Exos have the capacity to regulate the cellular phenotype, function, and homing mechanisms through their bioactive substances. They possess the unique ability to mitigate detrimental immune response, thereby promoting the survival and regeneration of parenchymal cells [21]. Exos represent a groundbreaking, cell-free therapeutic approach for PA. However, the challenge of rapid absorption by surrounding tissues in the dynamic local microenvironment of PA can undermine their efficacy [9]. To address this, the use of injectable hydrogels for the precise delivery of Exos offers an effective solution.

In this study, an injectable hydrogel (DCC) based on oxidized dextran (ODex) and carboxymethyl chitosan (CMCS) was prepared through a Schiff base reaction. This prepared injectable DCC hydrogel was utilized as both a physical barrier and a delivery vehicle for Exos to treat postoperative peritoneal adhesions (Scheme 1). It is anticipated that the DCC/Exo system will not only effectively cover the wound surface but also serve as a potent preventive measure against adhesions, effectively reducing apoptosis and inflammatory responses that are secondary to oxidative stress. We have also formulated a scientific hypothesis to elucidate the mechanisms behind the DCC/Exo system's exceptional anti-adhesion efficacy. 1) the prepared DCC hydrogels have excellent injectability and gelation properties, allowing complete coverage of the injured surface; 2) the DCC hydrogels can not only act as carriers for Exos but also may enhance their retention rate in the abdominal cavity, thereby optimizing the therapeutic efficacy of the Exos; and 3) the DCC/Exo system may modulate the microenvironment of damaged tissues by leveraging the antioxidant and anti-inflammatory properties of Exos, thereby potentially reducing excessive collagen deposition and promoting tissue repair. Therefore, we systematically investigated the injectability of DCC hydrogel and the controlled release behavior of Exos. Furthermore, the DCC/Exo system's therapeutic capabilities were thoroughly investigated in mice models *in vivo*, including its ROS scavenging properties, mitigation of oxidative stress-induced damage, reduction of inflammatory responses, and modulation of macrophage phenotypes.

2. Materials and methods

2.1. Animals, cell lines, and materials

All experimental animals were procured from the Laboratory Animal Center at North China University of Science and Technology. They were housed in a contamination-free environment with sterilized nutrition and water. All animal experiments were conducted humanely, following the National Research Council's Guide for the Care and Use of Laboratory Animals. These activities were all under the supervision and approval of the North China University of Science and Technology, and all animal experiments complied with the ARRIVE guidelines (Approval number: Beijing, SCXK 2019–0008). Human peritoneal mesothelial cells (HPMCs) and *RAW264.7* macrophage cells were obtained from the BeNa Culture Collection. Additionally, medical-grade sodium hyaluronate gel

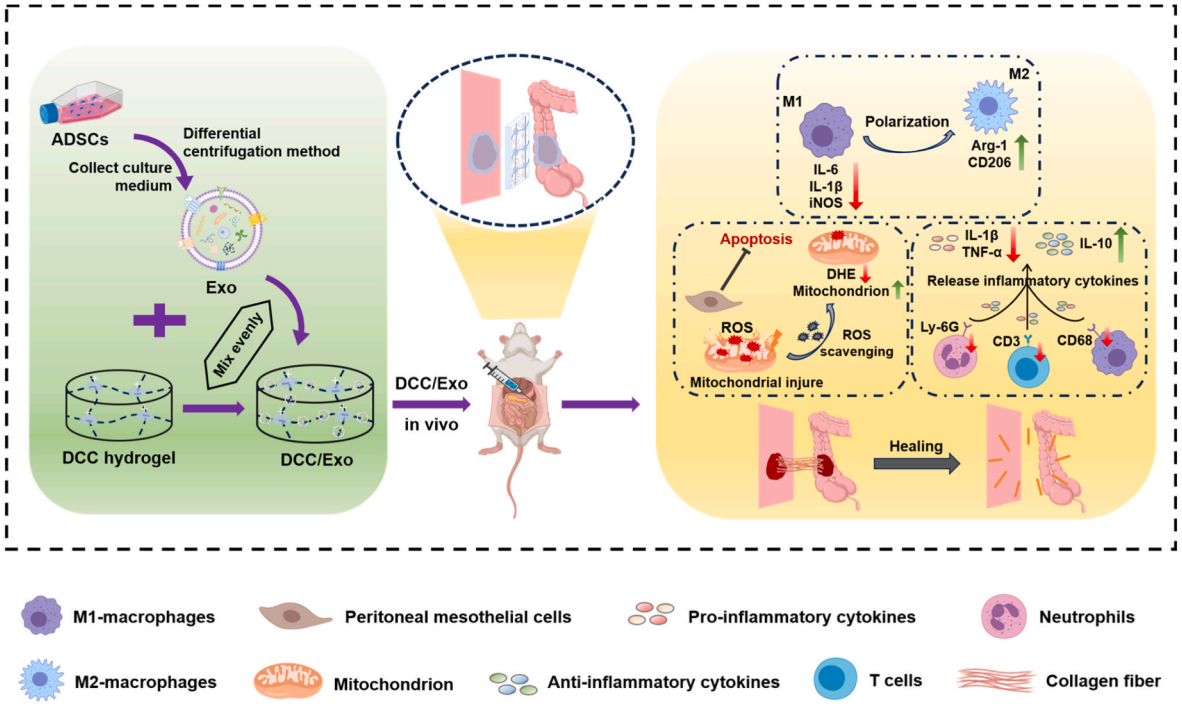

Schema.1. A schematic depiction of the combined approach using DCC hydrogel loaded exosomes aimed at the prevention of peritoneal adhesions.

(HA) was obtained from Hangzhou Xiehe Medical Supplies. Dextran with a molecular weight of 2×10^6 Da and carboxymethyl chitosan (a viscosity of 20 mPa s, a deacetylation degree of 85 %, and a carboxymethyl degree of 80 %) were acquired from Macklin Co. (Shanghai, China). All the other chemicals used in the experiment were supplied by Jiangtian Chemical Co. (Tianjin, China).

2.2. Preparation and characterization of DCC hydrogels

According to our previous study [22], aldehyde-modified dextran was synthesized by an oxidation reaction utilizing sodium periodate. Briefly, 3.96 g of dextran (0.01 mol) was dissolved in 50 mL of deionized water. Subsequently, 0.54 g of sodium periodate (0.0025 mol) was added to the dextran solution and the reaction was carried out in the dark. After 3 h, 3 mL of glycol was added to the mixed solution to terminate the reaction. Then, the reacted solution underwent dialysis against deionized water to obtain the oxidized dextran (ODex). The injectable oxidized dextran-carboxymethyl chitosan (DCC) hydrogels were prepared by thoroughly mixing equal proportions of ODex solution (5 wt%) and CMCS solution (5 wt%) [22].

The rheological behaviors of the DCC hydrogels were analyzed using a HAAKE MARS rheometer (USA). Dynamic storage modulus (G') and loss modulus (G'') measurements were measured at a frequency of 1 Hz and a constant strain of 1 %. Furthermore, the hydrogels were subjected to a step strain sweep at 37 °C and a frequency of 1 Hz with oscillatory strain amplitudes (γ) alternating from 1 % to 500 % and each strain interval lasting for 100 s. In addition, the injectability of the prepared hydrogels was evaluated using a conventional electromechanical tester (Si Pai Inc., China) equipped with a 50 N load cell. The syringe was securely fixed in a tensile grip, and the plunger was steadily depressed by an upper compressive plate according to previous report [23]. To determine the force required for injection, a 1 mL syringe fitted with an 18 G needle was utilized to extrude the hydrogels at a controlled flow rate of 1 mL min^{-1}.

2.3. Cytotoxicity assay

The cytotoxicity of the prepared DCC hydrogels were evaluated using HPMCs via the CCK-8 assay (Solarbio, China). Briefly, 1 g of DCC hydrogel was immersed in 10 mL of complete RPMI-1640 medium and incubated at 37 °C for 48 h to generate the hydrogel extract. Subsequently, the HPMCs were incubated with these extracts for 24 and 48 h, respectively. The HPMCs were cultured in RPMI-1640 complete medium as a control. Finally, their cell viability was determined using the CCK-8 assay and calculated according to Equation (1):

$$\text{Cell viability} = \frac{A_{sample} - A_{blank}}{A_{control} - A_{blank}} \times 100\ \% \quad (1)$$

The A_{sample} and $A_{control}$ are the absorbance values measured from the hydrogel extract and the control group, respectively. Additionally, A_{blank} indicates the absorbance of the CCK-8 solution under cell culture-free conditions.

In addition, cell morphology was observed by acridine orange/propidium iodide (AO/PI) staining (Baiolaibo, China). The fluorescent images were captured with a fluorescence inverted microscope (Nikon, Japan).

2.4. Subcutaneous implantation test

To track the distribution and persistence of the implanted DCC hydrogels, the DCC hydrogels were conjugated with Cy5-dextran and injected subcutaneously in a volume of 100 μL per mouse. Subsequently, fluorescence images were captured at intervals on days 1, 3, 5, 7, and 9 using an IVIS® Lumina imaging system (PerkinElmer, USA).

To assess the histocompatibility of the DCC hydrogels, six mice (25–30 g, 6 weeks old) were dorsally injected with 100 μL of DCC hydrogels. Tissue samples around the injection sites were collected on days 5 and 14 post-injection. The presence of neutrophil marker Ly6G (Cell Signaling Technology, USA) was detected by immunohistochemical staining.

2.5. Preparation and characterization of exosomes

Primary ADSCs were obtained from Sprague-Dawley (SD) rats (male, aged 3–4 weeks, weighing 80 ± 10 g) according to previous methods [24]. Exos were derived from the supernatants of ADSCs via differential centrifugation using an ultrahigh-speed centrifuge (Beckman Coulter, USA). The morphology and structural integrity of the isolated Exos were observed by transmission electron microscopy (TEM, Hitachi, Japan). Additionally, the particle size distribution of Exos was measured by nanoparticle tracking analysis (NTA, Malvern, UK). To further characterize the Exos, Western blot analysis was used to assess the expression of the key protein markers, including Alix (Wanleibio, China), TSG101 (Wanleibio, China), CD63 (Wanleibio, China) and Calnexin (Wanleibio, China).

2.6. In vivo tracing of DCC/Exo

Exos were fluorescently labeled in accordance with the manufacturer's protocol. Briefly, a 10 μM Dil solution (Beyotime, China) was added to PBS containing the Exos and incubated at room temperature for 30 min to facilitate labeling. To remove unbound dye, the labeled Exos were centrifuged at 100,000×*g* for 30 min at 4 °C. The Dil-labeled Exos were further isolated by ultracentrifugation at 130,000×*g* for 2 h and then mixed with the DCC hydrogel to produce DCC/Dil-labeled Exos. This prepared DCC/Dil-labeled Exos were injected into subcutaneous tissue of mice. Subsequently, the tissue was subjected to cryogenic sectioning using a Leica cryostat. The sections were examined by a laser scanning confocal microscope (Andor Dragonfly, Oxford Instruments, UK).

2.7. Release kinetics of exosomes from DCC hydrogels

A DCC hydrogel (100 μL) containing 30 μg of Exos was immersed in 200 μL of PBS at 37 °C. At set intervals, 100 μL of the release solution was removed, and an equal amount of fresh PBS was added. The release of Exos was determined over 8 days using a BCA protein assay kit (Solarbio, China).

2.8. Flow cytometry

To induce macrophage polarization *in vitro*, *RAW264.7* cells were first treated with 20 μg/mL Exos for 1 h, then exposed to lipopolysaccharides (LPS, Sigma-Aldrich, USA) at a concentration of 1 μg/mL [25]. After a coculture period of 12 h, the *RAW264.7* cells were stained with a Zombie NIR™ Fixable Viability Kit (BioLegend, USA). Before proceeding with immunostaining, to effectively block Fc receptors, the *RAW264.7* cells were preincubated with 1.0 μg of the TruStain FcX™ anti-mouse CD16/32 antibody (BioLegend, USA) in a 100 μL solution on ice for 5–10 min. *RAW264.7* cells were incubated in PBS buffer containing 2 % FBS at 4 °C for 30 min to stain the cell surface. Subsequently, directly conjugated antibodies against the following specific murine proteins were used: FITC-conjugated anti-mouse CD11b (BioLegend, USA), BV421-conjugated anti-mouse F4/80 (BioLegend, USA), and AF700-conjugated anti-mouse CD86 (BioLegend, USA). Intracellular labeling was performed with Fix Buffer (BioLegend, USA) to fix the cells. Then, the cells were permeabilized using a 10 × concentration of Intracellular Staining Permeabilization Wash Buffer (BioLegend, USA) and subsequently stained with APC-conjugated anti-mouse CD206 (BioLegend, USA). Finally, flow cytometric analysis was performed using a 21-color CytoFLEX (Beckman Coulter, USA) instrument to acquire the data. The data were analyzed by CytoExpert (Beckman

Coulter, USA) and FlowJo (Tree Star).

2.9. Assessing the anti-adhesion impact of DCC/Exo in vivo

The mouse peritoneal adhesion model was prepared according to our previous report [4]. Briefly, the KM mice were anesthetized with 2.5 % Avertin (0.095 mL/10 g) intraperitoneally, and the abdominal skin was prepared and disinfected. The cecum injury was induced by dry gauze abrasion until petechial hemorrhage appeared, and a 1 × 1 cm^2 wound was made on the abdominal wall with a scalpel. The mice were divided into 4 groups ($n = 5$), including the control group, commercial sodium hyaluronate (HA) hydrogel group, DCC hydrogel group and DCC/Exo hydrogel group. The injured sites were covered with 100 μL of HA hydrogel, 100 μL of 2.5 wt% DCC hydrogel [22]. In the DCC/Exo group, 100 μL of DCC hydrogel, encapsulating 30 μg of Exos (30 μg/100 μL) was injected at the injured site [26]. For the control group, 100 μL of PBS was used to clean the injured cecum and abdominal wall. The adhesions on days 7 and 14 after surgery were assessed using a double anonymous method to score the model animals. The scoring criteria were as follows: 0, no adhesions; 1, one thin adhesion, loose and easily separated; 2, one or more thin adhesions; 3, relatively tight adhesions; 4, one or more tight adhesions; and 5, large area of vascularized adhesions.

2.10. RNA sequencing (RNA-seq) and data analysis

To compare the gene expression levels between the DCC hydrogel and DCC/Exo groups, RNA-seq was performed by Novogene Bioinformatics Technology Corp., Ltd. (Beijing, China). Subsequently, Gene Ontology (GO) functional enrichment, Kyoto Encyclopedia of Genes and Genomes (KEGG) pathway and Reactome enrichment analysis of differentially expressed genes (DEGs) were conducted with clusterProfiler software.

2.11. Immunohistochemical and immunofluorescence staining

Mice were euthanized at different time points after surgery, followed by the rapid excision of cecum and abdominal wall tissues. The collected tissue samples were fixed and embedded in paraffin for further analysis. Apoptosis at the wound site was detected using the terminal deoxynucleotidyl transferase (TdT)-mediated dUTP-biotin nick end labeling (TUNEL) staining (Shanghai Life-ILab Biotech Co., Ltd., China) according to the manufacturer's protocol. To evaluate the inflammatory response, specific antibodies were selected for staining: Anti-Ly6G (Cell Signaling Technology, USA), anti-CD3 (Abcam, UK), and anti-CD68 (Cell Signaling Technology, USA). Fibrosis was assessed by Masson trichrome (Leagene Biotechnology, China) and Sirius red (Leagene Biotechnology, China) staining [27]. These stained images were captured by an optical microscope (Olympus, Japan).

Optimum cutting temperature (OCT) tissue sections at 1 d after peritoneal injury were used to detect reactive oxygen species (ROS) levels. The ROS levels were evaluated using dihydroethidium (DHE, Cayman Chemical, USA). Additionally, MitoTracker Red (Invitrogen, USA) was used to label mitochondria to observe mitochondrial damage.

Antibodies against iNOS (Santa Cruz Biotechnology, USA) and CD206 (Cell Signaling Technology, USA) were used as markers to observe macrophage polarization. For immunofluorescence detection, the following fluorescent secondary antibodies were used: anti-mouse AF568 (Thermo Fisher, USA) and anti-rabbit AF488 (Thermo Fisher, USA). Nuclear staining was performed using 4′, 6′-Diamidino-2-phenylindole (DAPI) (Cell Signaling Technology, USA). The high-speed confocal microscope (Oxford Instruments, UK) was used to capture the resulting fluorescence images. All the images were quantitatively analyzed with ImageJ software.

2.12. Western blot

For total protein extraction, Radio Immuno Precipitation Assay (RIPA) lysis buffer (Solarbio, China) supplemented with 1 mM phenylmethanesulfonyl fluoride (PMSF) was used. Protein concentrations were quantified using a BCA kit (Solarbio, China). After separation by SDS–PAGE, proteins were transferred onto PVDF membranes (Millipore, USA). After 2 h, the membranes were blocked with 5 % skim milk and then incubated at 4 °C overnight with specific primary antibodies, including those specific for interleukin-6 (IL-6, Wanleibio, China), Arginase-1 (Arg-1, Proteintech, USA), and GAPDH (Proteintech, USA). Afterward, the membranes were incubated for another 2 h with secondary antibodies at room temperature and were finally visualized with enhanced chemiluminescence (ECL) solution (Epizyme Biomedical Technology, China).

2.13. Enzyme-linked immunosorbent assay (ELISA)

Following the establishment of PA model and treated by hydrogels and Exos, serum samples were systematically collected from the mice at predefined time points: 0, 1, and 5 days. The serum levels of IL-1β, tumor necrosis factor-α (TNF-α), and IL-10 were measured using ELISA kits from ABclonal Biotechnology Co., Ltd. (Wuhan, China).

2.14. Statistical analysis

The data are presented as the means ± standard errors. One-way ANOVA was used for group comparisons and the least significant difference (LSD) test was used for two-way comparisons. Statistical processing was carried out with GraphPad Prism 9 and ImageJ, with a $P < 0.05$ indicating statistical significance.

3. Results

3.1. Formation and characteristics of the DCC hydrogels

Many biodegradable and injectable hydrogels have been engineered to mitigate postoperative abdominal adhesions [28,29]. In this study, a biodegradable and injectable DCC hydrogel was prepared via a Schiff base reaction between the aldehyde group of ODex and the amino group of CMCS (Fig. 1A). When ODex was mixed with the CMCS solution, it exhibited a homogeneous sol state with the G' being lower than the G''. As the reaction progressed, both G' and G'' increased. The intersection of these moduli indicated the gelation time of the DCC hydrogels. Eventually, G' surpassed G'', stabilized, and indicated the formation of the hydrogels (Fig. 1B). The gelation dynamics of DCC hydrogels with different mass ratios of ODex and CMCS were thoroughly examined. Fig. 1C & S1 showed that the gelation time decreased from 178 s to 121 s when the ODex/CMCS mass ratio changed from 1:2 to 1:0.5. Meanwhile, G' gradually increased from 76 Pa to 112 Pa, and this change was attributed to the increased crosslinking density caused by a higher concentration of aldehyde groups in the DCC hydrogel (2:1). The DCC hydrogel exhibited injectability through reversible dynamic chemical crosslinking via imine bonds. The mixture of the ODex and CMCS solution was injected easily by a syringe, indicating that DCC hydrogels have favorable injectability (Fig. 1D). The viscosity of DCC hydrogel decreased significantly when it was extruded through a syringe needle. Additionally, the force applied when the DCC hydrogel was injected through an 18 G clinical needle at a flow rate of 1 mL/min was recorded (Fig. 1E), and the results showed an initial linear and then a plateau (Fig. S2). Regardless of the ODex/CMCS mass ratio, the injection forces in all cases were less than 1 N. This measurement represented the force applied by physicians to initiate and maintain plunger movement. Overall, this procedure greatly simplifies the difficulty of the operation. In addition, the prepared DCC hydrogel showed good tissue adhesive property. As shown in Figs. S3 and S4, the adhesive strength of the DCC

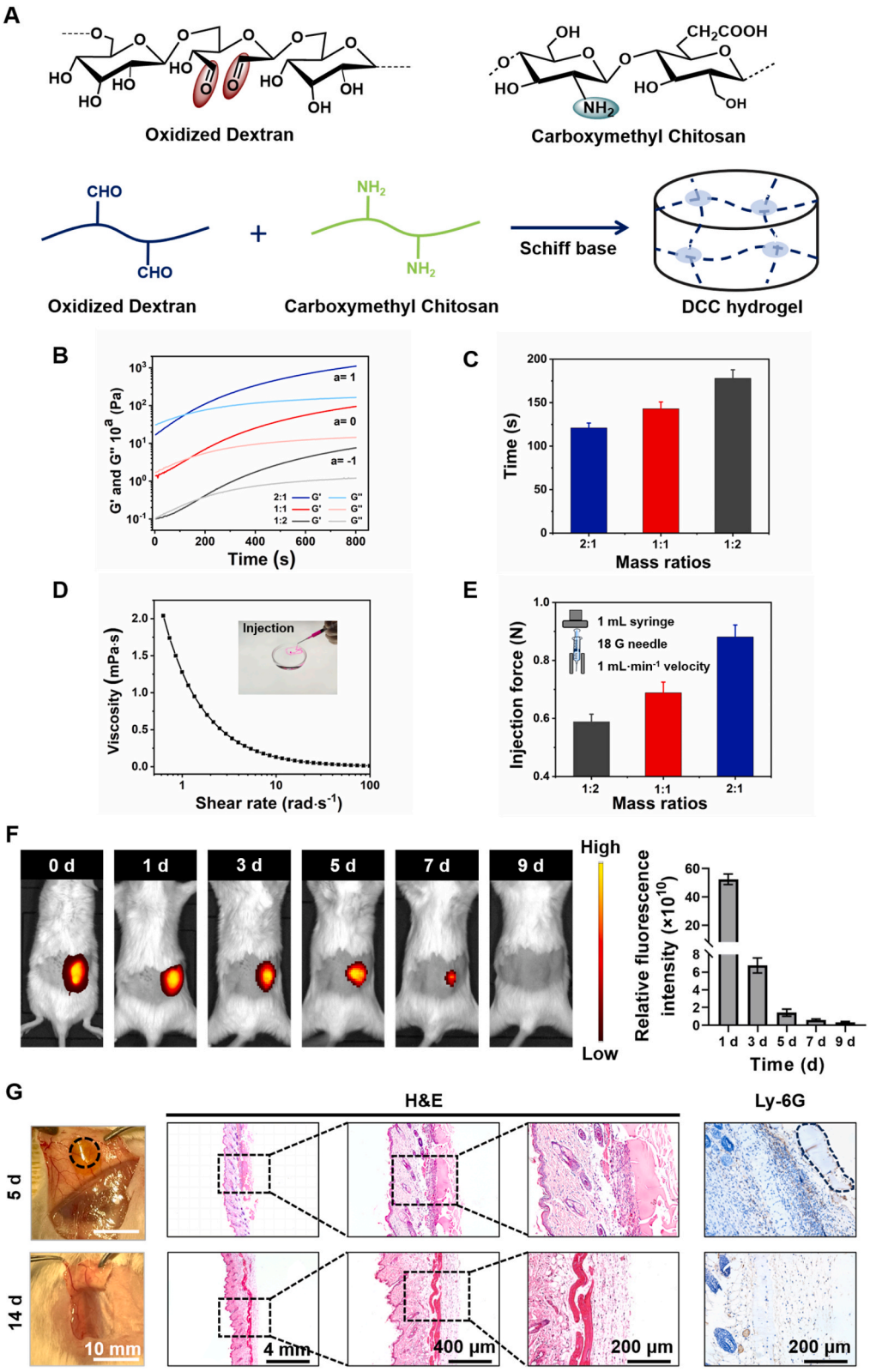

Fig. 1. Formation and characteristics of the DCC hydrogels. (A) Schematic of the preparation of the DCC hydrogels. (B) The gelation kinetics of the DCC hydrogels were analyzed via rheological oscillation time sweeps ($n = 3$). (C) Measurement of gelation time ($n = 3$). (D) The shear-thinning properties of the DCC hydrogels were examined through viscosity-shear rate assessments ($n = 3$). (E) The force needed to extrude the hydrogels by a 1 mL syringe with an 18G needle at a rate of 1 mL min^{-1} was recorded. The average force, measured during the steady phase of the force–displacement curve, represented this injection force ($n = 3$). (F) Fluorescence image of hydrogels implanted subcutaneously and the ratio of fluorescence intensity on days 1, 3, 5, 7, and 9 to fluorescence intensity on day 0 ($n = 3$). (G) Histological observations of the DCC hydrogels on days 5 and 14 following subcutaneous injection ($n = 3$).

hydrogel on skin surface was 7.7 kPa. Moreover, the DCC hydrogel can adhere on various tissue surface without the need for additional surface treatments, thus simplifying the application process.

To analyze degradability *in vivo*, DCC hydrogels labeled with Cy5 were implanted subcutaneously. As shown in Fig. 1F, fluorescence imaging utilizing the IVIS living imaging system revealed clear signals in the dorsal area immediately after injection (day 0), indicating rapid formation of the DCC hydrogels *in situ*. Over time, the fluorescence signal remained at the injection site, indicating the robust integrity of the hydrogel. Additionally, the fluorescence intensity decreased significantly on day 7, suggesting that the DCC hydrogels degraded gradually over time *in vivo*. The appropriate retention time of the DCC hydrogel is an important factor in preventing adhesion, and its ability to degrade within a specific time is also beneficial to tissue healing. In contrast, the commercial HA hydrogels degraded faster than the DCC hydrogels *in vivo*, and no fluorescent signal was observed on day 5 after injection (Fig. S7).

The prepared DCC hydrogel showed good biocompatibility. As shown in Fig. S5, the HPMCs survival rates in the DCC group were comparable to those in the normal group after 24 and 48 h of incubation, reaching approximately 100 %. In addition, most of the HPMCs fluoresced in green, and little dead HPMCs fluoresced in red (Fig. S6), indicating that DCC hydrogels have no cytotoxic effects.

As shown in Fig. 1G, residual DCC hydrogels were detected in the subcutaneous tissue on day 5 post-implantation. On day 14, these hydrogels had completely degraded, which was consistent with the results from *in vivo* imaging results. In addition, on day 5, a slight inflammatory response was marked by the presence of $Ly6G^+$ neutrophils. As the hydrogel degraded, the presence of $Ly6G^+$ neutrophils was minimal on day 14.

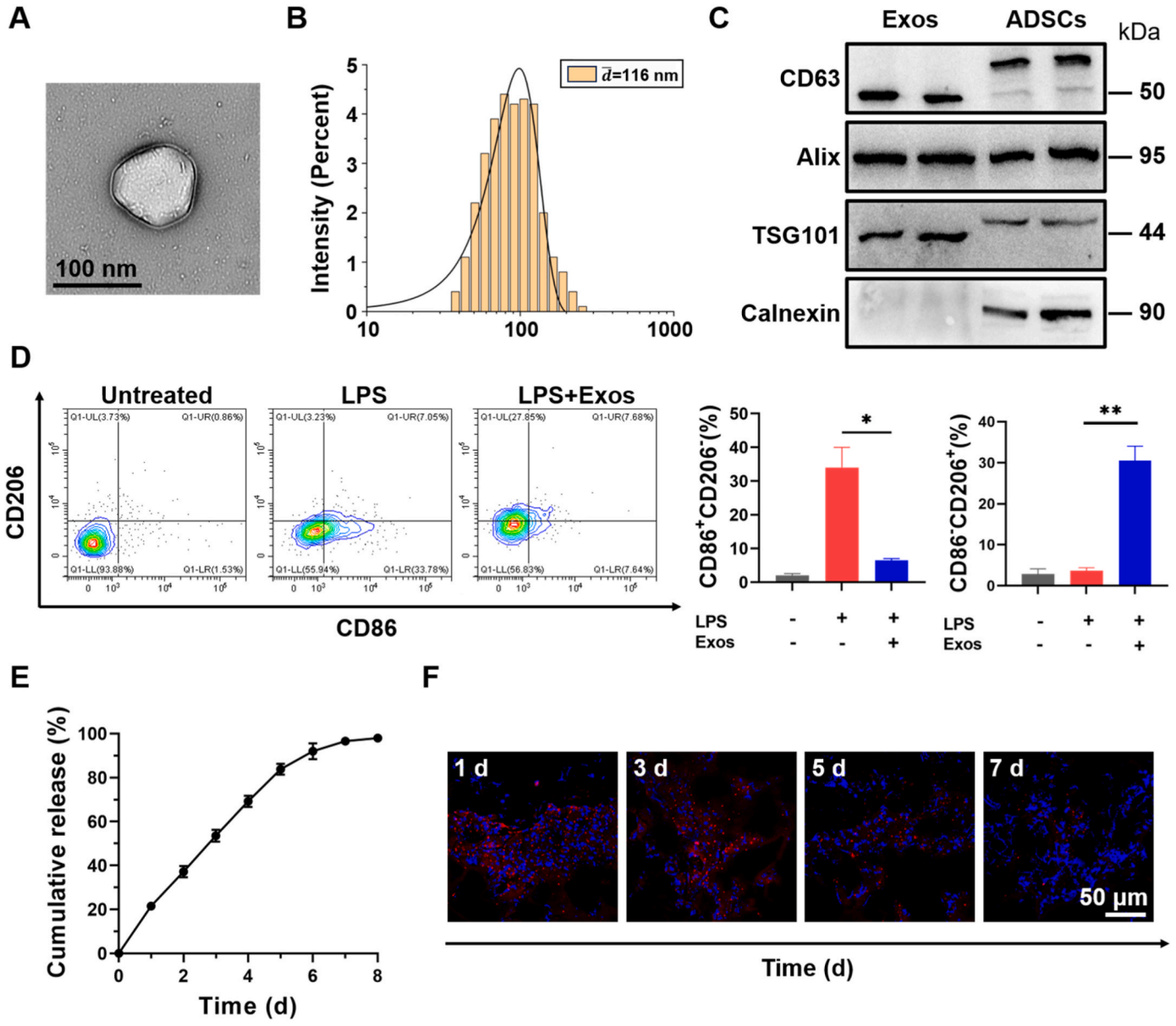

Fig. 2. Preparation and release of exosomes from DCC hydrogels *in vitro* and *in vivo*. (A) A characteristic TEM image of an Exo. (B) Analysis of Exos particle sizes. (C) Western blot of CD63, Alix, TSG101, and Calnexin. (D) Flow cytometry data showing CD86 and CD206 expression in LPS- and Exos-treated *RAW264.7* cells ($n = 3$, $^*p < 0.05$, $^{**}p < 0.01$). (E) Cumulative Exos release from the DCC hydrogels over an 8-day period ($n = 3$). (F) Fluorescence staining-based tracking of DCC/Dil-labeled Exos implanted *in vivo*.

3.2. Preparation and release of exosomes from DCC hydrogels in vitro and in vivo

To obtain Exos, a simple and effective method was used to purify Exos by differential centrifugation (Fig. S8). TEM images revealed that the Exos had a cup-shaped, double-membrane structure (Fig. 2A) with an average size of 116 nm (Fig. 2B). Typical proteins including CD63, Alix, and TSG101 were present at high levels, whereas an endoplasmic reticulum marker Calnexin was absent (Fig. 2C). Overall, these results validated the effective preparation of ADSCs-derived Exos.

M1 and M2 macrophage polarization play a vital role in injury response [30]. To explore the regulatory effects of Exos on macrophages, LPS-stimulated *RAW264.7* cells were treated with Exos to investigate macrophage regulation (Fig. 2D). The percentage of M1 ($CD86^{+}$) macrophages in the Exos-treated group was significantly lower than that in the LPS-stimulated group. However, there was a substantially greater percentage of M2 ($CD206^{+}$) macrophages, and the difference was statistically significant ($p < 0.01$). These results indicated that Exos mitigate LPS-induced inflammatory responses and promote macrophage polarization towards the M2 phenotype.

To examine Exos release characteristics from DCC hydrogels *in vitro*, 30 μg of Exos were loaded into 100 μg of DCC hydrogels. As shown in Fig. 2E, the majority of Exos were sustained within the DCC hydrogel for up to 8 days, demonstrating a sustained release profile. This gradual release pattern mitigated the burst release phenomenon typically associated with Exos delivery, thereby enhancing their stability and potentially their therapeutic efficacy. During this period, more than 95 % of the Exos were released. Their combined synergistic effect enhances the therapeutic efficacy.

To track the binding and persistence of Exos *in vivo*, subcutaneous implantation of DCC/Dil-labeled Exos was performed, followed by fluorescence tracking at different intervals (Fig. 2F). Notably, a lot of Dil-labeled Exos appeared on day 1 after transplantation. However, the presence of these Exos decreased significantly on days 3 and 5, and red fluorescence was barely detectable on day 7. This trend suggested that the main activity of DCC/Exo occurred in the initial phase of tissue injury.

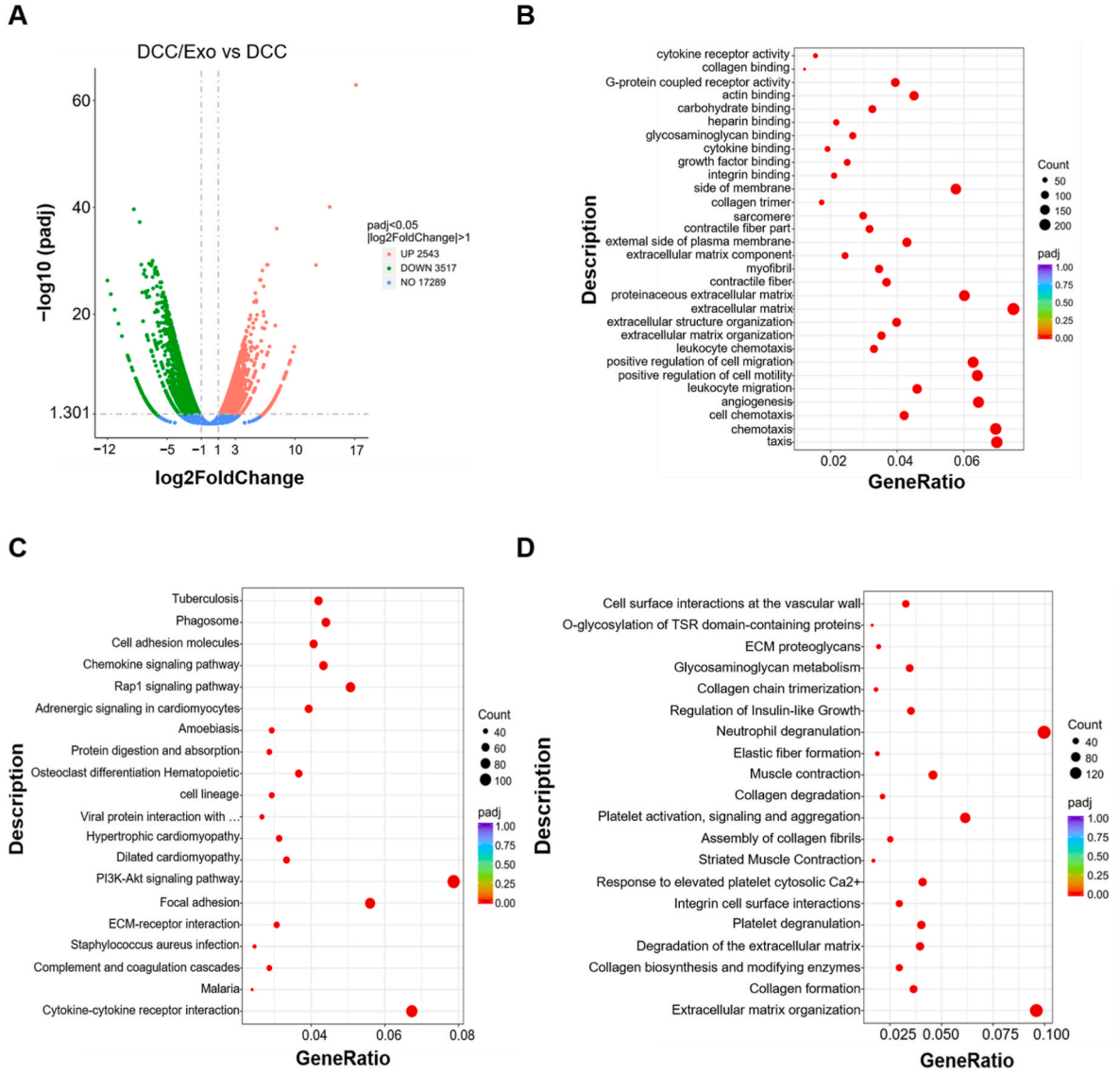

Fig. 3. The effects of DCC/Exo on the gene expression level *in vivo* ($n = 3$, the DCC vs DCC/Exo groups). (A) Differential gene volcano mapping analysis. (B) Scatterplot analysis for GO functional enrichment of downregulated differentially expressed genes (DEGs). (C) KEGG pathway enrichment scatterplot analysis of downregulated DEGs. (D) Reactome enrichment analysis scatterplot of downregulated DEGs.

3.3. The effects of DCC/Exo on the gene expression level in vivo

To explore the potential mechanism of DCC/Exo on PA repair, the tissue samples were harvested from mice in the DCC group and the DCC/Exo group on day 5 post-treatment. RNA-seq was subsequently performed to analyze the differential gene expression profiles and enrichment scenarios between the groups.

As illustrated in the volcano plot, a comprehensive transcriptomic analysis revealed significant differential gene expression between the DCC/Exo group and the DCC group. Specifically, 6060 genes exhibited a statistically significant change in expression levels between the DCC/Exo and DCC group. Among these, 2543 genes were significantly upregulated (the red dots), and 3517 genes were significantly downregulated (the green dots) in DCC/Exo group (Fig. 3A). GO analysis indicated that the downregulated DEGs are mainly involved in the formation of the extracellular matrix, proteinaceous extracellular matrix, and contractile fibers. The molecular functions predominantly included integrin binding, growth factor binding, and cytokine binding, which are involved in biological processes of chemotaxis, angiogenesis, and leukocyte migration (Fig. 3B & S9, $p < 0.05$). KEGG pathway enrichment analysis revealed that 20 pathways associated with the downregulated genes, suggesting that the DCC/Exo exerted a preventative effect on PA through multiple pathways. Compared with the DCC group, the DCC/Exo group exhibited significant downregulation of several key pathways ($p < 0.05$), including the PI3K-Akt signaling pathway, cytokine-cytokine receptor interaction, focal adhesion, Rap1 signaling pathway, and ECM-receptor interaction pathway ((Fig. 3C). These results suggested that the introduction of Exos may modulate the physiological effects through

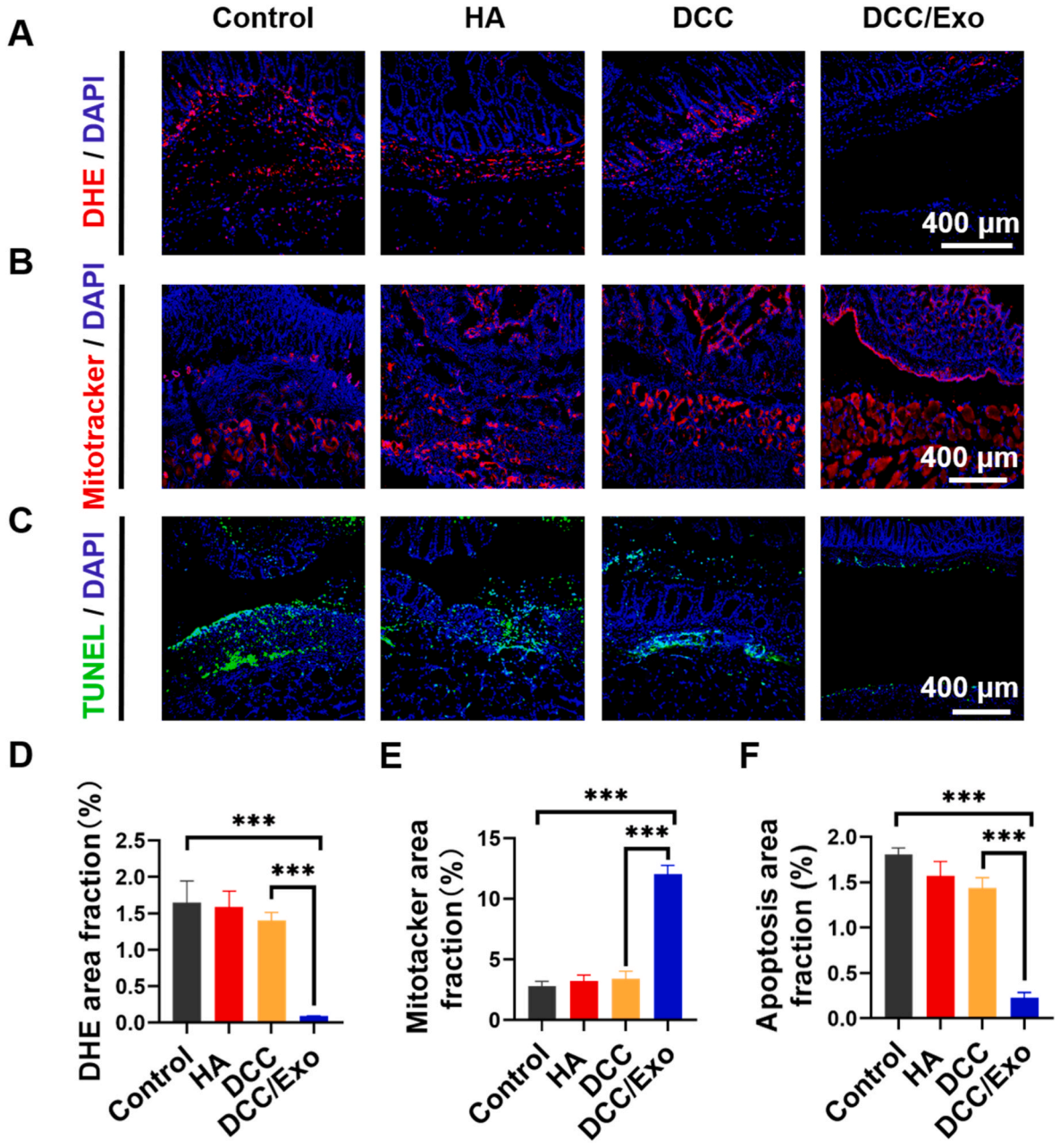

Fig. 4. The suppressive effects of DCC/Exo on oxidative stress and mitochondrial damage ($n = 3$, $^{*}p < 0.05$, $^{**}p < 0.01$, $^{***}p < 0.001$). (A) DHE buildup (red fluorescence) in adhesion tissues on day 1 after injury. (B) Representative images of the adhesion of mitochondria (red fluorescence) after peritoneal injury on day 1. (C) TUNEL staining images revealed the presence of apoptotic cells on day 1. (D–F) Quantitative histograms of DHE, mitochondria and apoptotic cells. (For interpretation of the references to color in this figure legend, the reader is referred to the Web version of this article.)

these pathways.

Analysis utilizing the Reactome database (Fig. 3D) indicated that, relative to the DCC group, the DCC/Exo group exhibited significant downregulation of genes related to collagen formation, extracellular matrix organization, integrin-related pathways and neutrophil degranulation. Taken together, these results confirmed that DCC/Exo can modulate the immune microenvironment post-adhesion by downregulating the expression of inflammation-related genes and pathways, thereby preventing adhesion.

3.4. The suppressive effects of DCC/Exo on oxidative stress and mitochondrial damage

Surgical injury can trigger an excessive production of ROS, including superoxide anions and hydroxyl radicals [31]. The production of these free radicals is a potential pathogenic factor contributing to the formation of PA and they can act as a signaling molecule to exacerbate the inflammatory response and promote the release of proinflammatory cytokines by immune cells [32–34]. To assess the antioxidant effects of DCC/Exo hydrogels *in vivo*, their radical scavenging and anti-apoptosis properties were investigated. As shown in Fig. 4A, on day 1, a significant amount of red DHE fluorescence was observed around the cell nuclei in the control, HA, and DCC groups. Notably, the strongest red fluorescence appeared in the control group, particularly in the adhesion area between the cecum and abdominal wall. As expected, almost no DHE fluorescence can be observed after treatment by DCC/Exo, and the average red fluorescence area fraction was reduced by 93.6 % compared to the DCC group (***$p < 0.001$). The fluorescence area fraction of the DCC/Exo was significantly lower than that of the other groups (Fig. 4D).

The DCC/Exo protected mitochondria from damage. As shown in Fig. 4B, the red fluorescence of MitoTracker mitochondria in the control group significantly decreased in the adhesion tissues compared to the healthy tissue (Fig. S10), indicating that the mitochondria are damaged by oxidative stress. As expected, the MitoTracker fluorescence significantly increased in the DCC/Exo group, and its average fluorescence was approximately 255 % higher than that of the DCC group (***$p < 0.001$, Fig. 4E). These results indicated that the DCC/Exo group effectively suppressed the oxidative stress damage to mitochondria, which is essential for maintaining cellular homeostasis. In addition, the DCC/Exo can also suppress the apoptosis in damaged tissue. Many TUNEL-positive cells were observed in the control group owing to oxidative stress damage. The HA and DCC groups showed a slight decrease in apoptosis. However, the numbers of apoptotic cells in the DCC/Exo group were significantly lower compared with the control group (***$p < 0.001$). This reduction was quantified by a decrease in the green fluorescence area fraction from 1.81 ± 0.07 % to 0.23 ± 0.06 %, indicating the effectiveness of synergistic treatment with Exos (Fig. 4C and F).

3.5. The effects of DCC/Exo on inflammatory microenvironment of peritoneal adhesions

Irritation and damage to the peritoneum (Fig. S11) lead to increased capillary permeability, followed by leakage of inflammatory cells and fibrin from the bloodstream into the peritoneal cavity. This process triggers inflammation and further results in adhesion. Minimizing inflammatory reactions and the accumulation of collagen fibers can prevent adhesion development. In this study, the inflammatory response and the incidence of early adhesions were assessed on day 5 after surgery. Notably, PA were distinctly apparent in the control group, whereas no adhesions were observed in the DCC/Exo group (Fig. 5A). In addition, Ly6G, CD3 and CD68 were selected as markers for inflammatory cells. The control group exhibited marked infiltration of $Ly6G^+$ cells (a neutrophils marker), $CD3^+$ cells (a T lymphocytes marker), and $CD68^+$ cells (a macrophages marker). The adhesive tissue in both the HA and DCC hydrogel groups was less dense than those in the control group. Additionally, the level of inflammation in the injured areas showed a slight decrease in the two hydrogel groups. As expected, the infiltration of neutrophils, T lymphocytes, and macrophages in the DCC/Exo group was significantly lower than those in the control (***$p < 0.001$) and DCC groups (*$p < 0.05$ or **$p < 0.01$, Fig. 5B–**D**). Similarly, when compared with the control group, there was a significant reduction in the levels of the proinflammatory cytokines IL-1β and TNF-α in the DCC/Exo group (***$p < 0.001$). Conversely, the level of IL-10 (an anti-inflammatory cytokine) was increased by DCC/Exo treatment (***$p < 0.001$). This increase was pronounced on day 1 and was sustained through day 5, the levels of IL-10 remained elevated in the DCC/Exo group compared to the control group.

These findings indicated that DCC/Exo diminishes the recruitment of inflammatory cells and the release of inflammatory mediators, inhibiting the activation of the inflammatory microenvironment and thereby preventing the formation of adhesions. Furthermore, regulation of the inflammatory microenvironment promoted the regulation of immune cells and enhance the activity of cellular repair, thereby facilitating tissue repair, these results are consistent with the previous report [35].

3.6. The effects of DCC/Exo on the macrophage polarization in vivo

Given the encouraging results of reduced local inflammatory cell infiltration and increased serum levels of anti-inflammatory cytokines after DCC/Exo treatment, the underlying mechanisms were investigated.

Macrophage polarization is recognized as a pivotal factor in modulating inflammatory response and tissue healing [36]. Many studies have shown that Exos can promote macrophage polarization, leading to elevated levels of anti-inflammatory cytokines and chemokines. This promotion is instrumental in reducing inflammation and aids tissue healing [37]. As shown in Fig. 6A and B, the quantity of iNOS-labeled M1 macrophages was significantly higher in the control group compared to the DCC/Exo group (***$p < 0.001$) on day 5. In contrast, the prevalence of M2 macrophages labeled with CD206 sequentially increased in the HA, DCC, and DCC/Exo groups (***$p < 0.001$) (Fig. 6A and C), and many M2 macrophages appeared in both the cecal and abdominal regions in the DCC/Exo group. Based on the average area fraction of M1 and M2 markers in each group, M2 macrophages in the DCC/Exo group accounted for the largest proportion of macrophages (Fig. 6D). In comparison, the number of proinflammatory M1 macrophages was notably decreased. The results suggest that DCC/Exo can inhibit the polarization of macrophages towards the proinflammatory M1 phenotype and instead promote their polarization towards the anti-inflammatory M2 phenotype.

To further investigate this effect, we conducted a detailed investigation of the secretion profiles of proinflammatory factors by M1 macrophages, including IL-1β, IL-6, and TNF-α, as well as the anti-inflammatory agents produced by M2 macrophages, which include Arg-1 and IL-10 via Western blotting [38]. As shown in Fig. 6E–**G**, compared to the control group, the M1-associated proteins IL-1β and IL-6 were downregulated in the DCC/Exo group. Conversely, a notable upregulation of the M2-specific protein Arg-1 was observed in the DCC/Exo group, with expression levels significantly higher than those in both the control and the DCC hydrogel groups (*$p < 0.05$) (Fig. 6E and H).

3.7. Anti-adhesion effects of the DCC/Exo

A prolonged inflammatory response can significantly interfere with the fibrinolytic system and the remodeling of the extracellular matrix at the site of injury. This fibrotic process is key to the pathology of PA [39, 40]. The formation of fibers and collagen is a way of repairing peritoneum after injury and occurs in the final stages of postoperative PA development [2]. To assess the anti-adhesion effect of the DCC/Exo system, injured tissues were collected on days 7 and 14 after surgery. The collected samples were examined for the presence of adhesions and

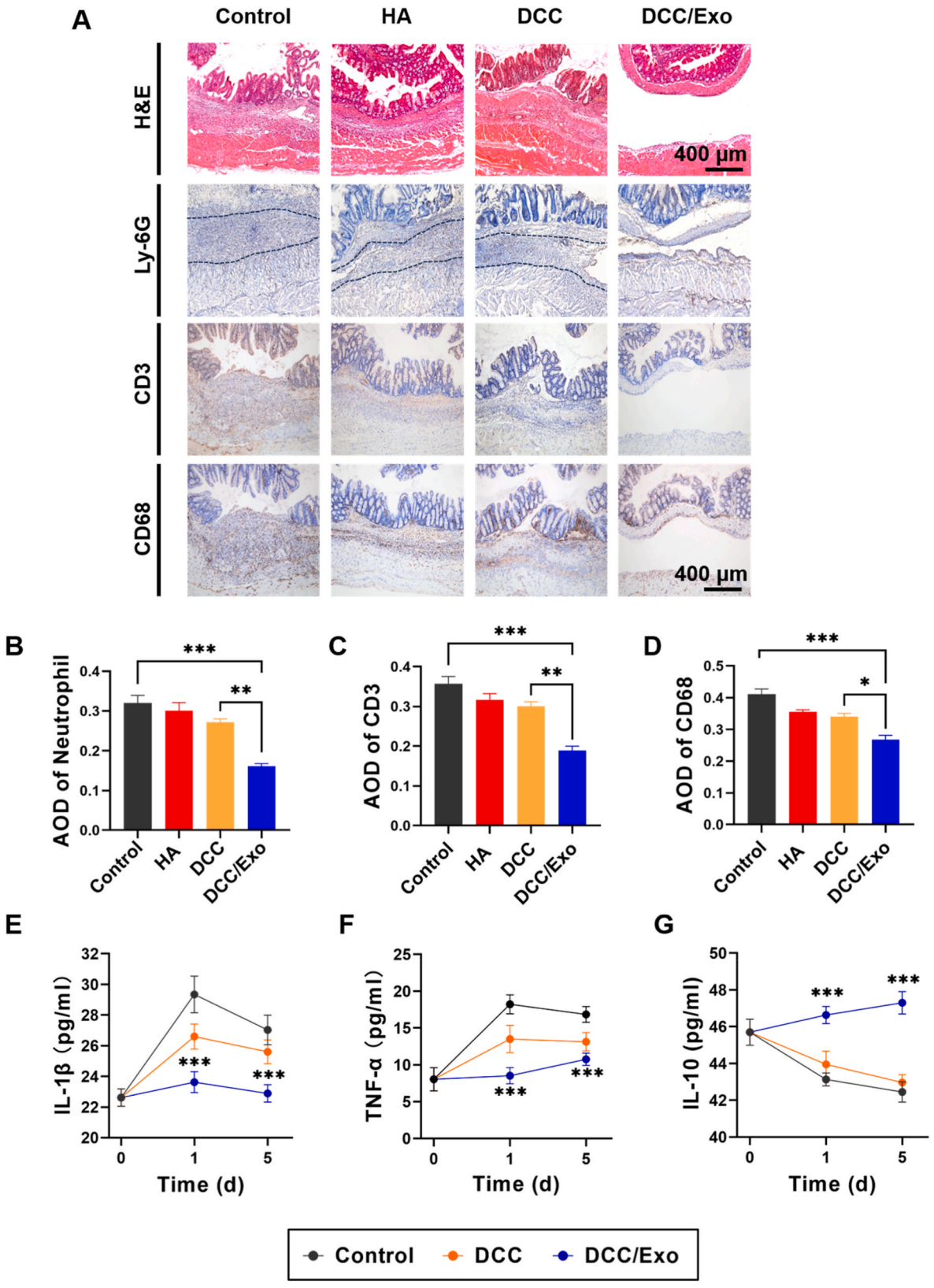

Fig. 5. The effects of DCC/Exo on inflammatory microenvironment of peritoneal adhesions. (A) H&E and immunohistochemical staining images of Ly6G, CD3, and CD68 on day 5 after surgery. (B–D) Quantitative analysis of Ly6G, CD3 and CD68 expression levels ($n = 3$, $^{*}p < 0.05$, $^{**}p < 0.01$, $^{***}p < 0.001$). (E–G) Serum levels of IL-1β, TNF-α, and IL-10 on days 0, 1, and 5 ($n = 3$, the DCC/Exo *vs* control, $^{***}p < 0.001$).

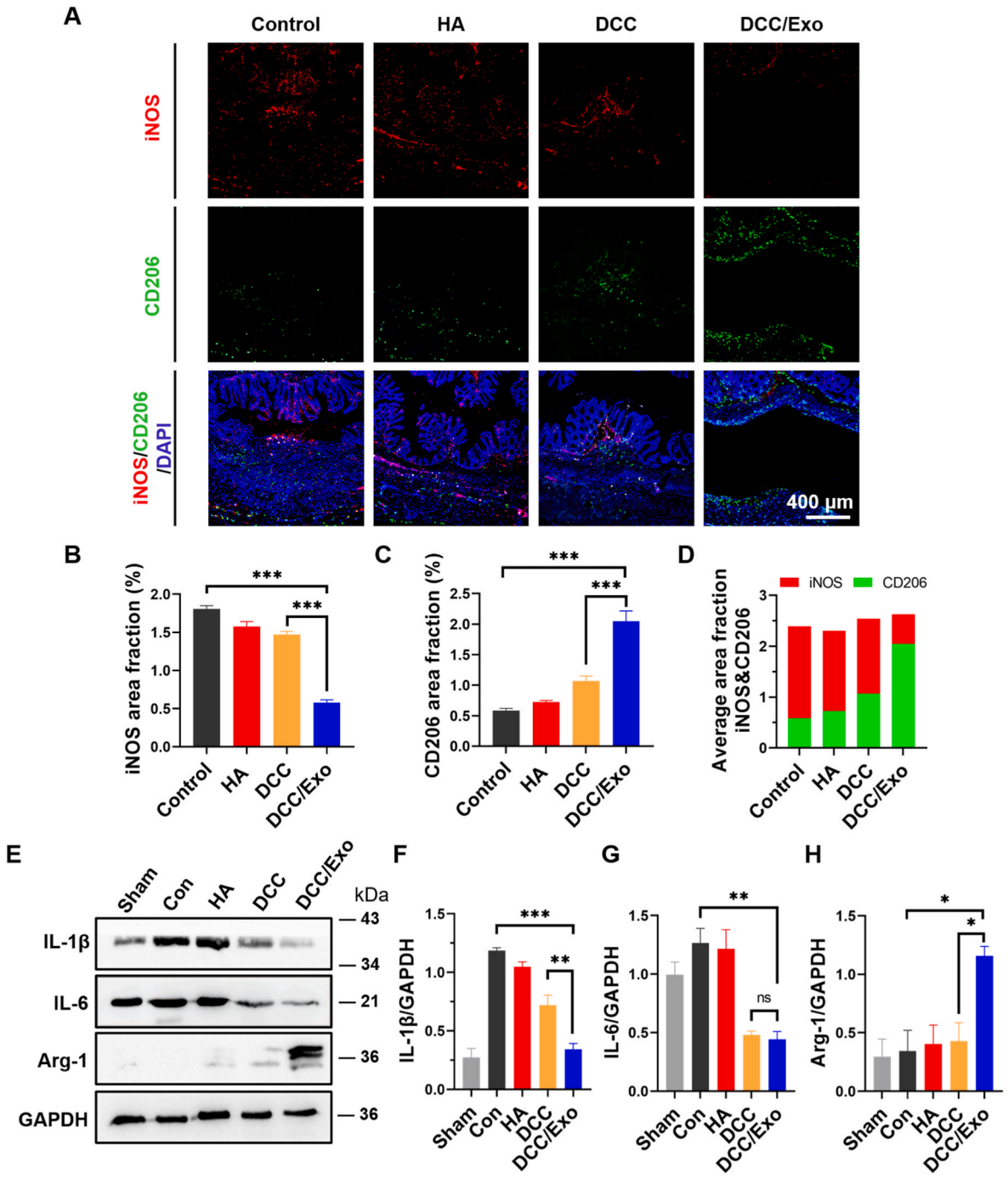

Fig. 6. The effects of DCC/Exo on the macrophage polarization *in vivo*. (A) iNOS (red) and CD206 (green) staining ($n = 4$). (B) The iNOS area fraction. (C) The CD206 area fraction. (D) Average area fractions of iNOS and CD206-positive cells. (E) Western blot analysis of IL-1β, IL-6 and Arg-1 in the various groups. (F–H) Quantification of the protein levels of IL-1β, IL-6, and Arg-1 ($n = 3$). (*$p < 0.05$, **$p < 0.01$, ***$p < 0.001$). (For interpretation of the references to color in this figure legend, the reader is referred to the Web version of this article.)

subsequently quantified using a standardized scoring system of adhesions. As shown in Fig. 7A and B, on day 7 post-surgery, distinct adhesions had formed between the abdominal wall epithelium and the cecum injury surface in the control group, and the adhesions became tighter and denser as the disease progressed on day 14. Correspondingly, the adhesion score in the control group increased from 3.6 points on day 7 to 4.6 points on day 14. More optimistically, the application of HA and DCC hydrogels led to a slight decrease in adhesion compared to the control group. Specifically, the adhesion scores for the HA group were 3.2 points on day 7 and 3.8 points on day 14, while the DCC group exhibited even lower scores of 2.4 points on day 7 and 3.2 points on day 14. These scores were significantly lower than those of the control group (**$p < 0.05$). In contrast, no adhesions were observed in the DCC/Exo group on days 7 and 14 after surgery. The cecum surface and the abdominal wall healed smoothly in the DCC/Exo group, with adhesion scores of 0 on day 7 and 0.2 on day 14, which was significantly lower than those in the control group (***$p < 0.001$). H&E staining images showed similar results. As shown in Fig. 7C, the adhesions area and thickness of the control group gradually increased with the progression of the disease. The adhesions involved the entire intestinal wall with dense connective

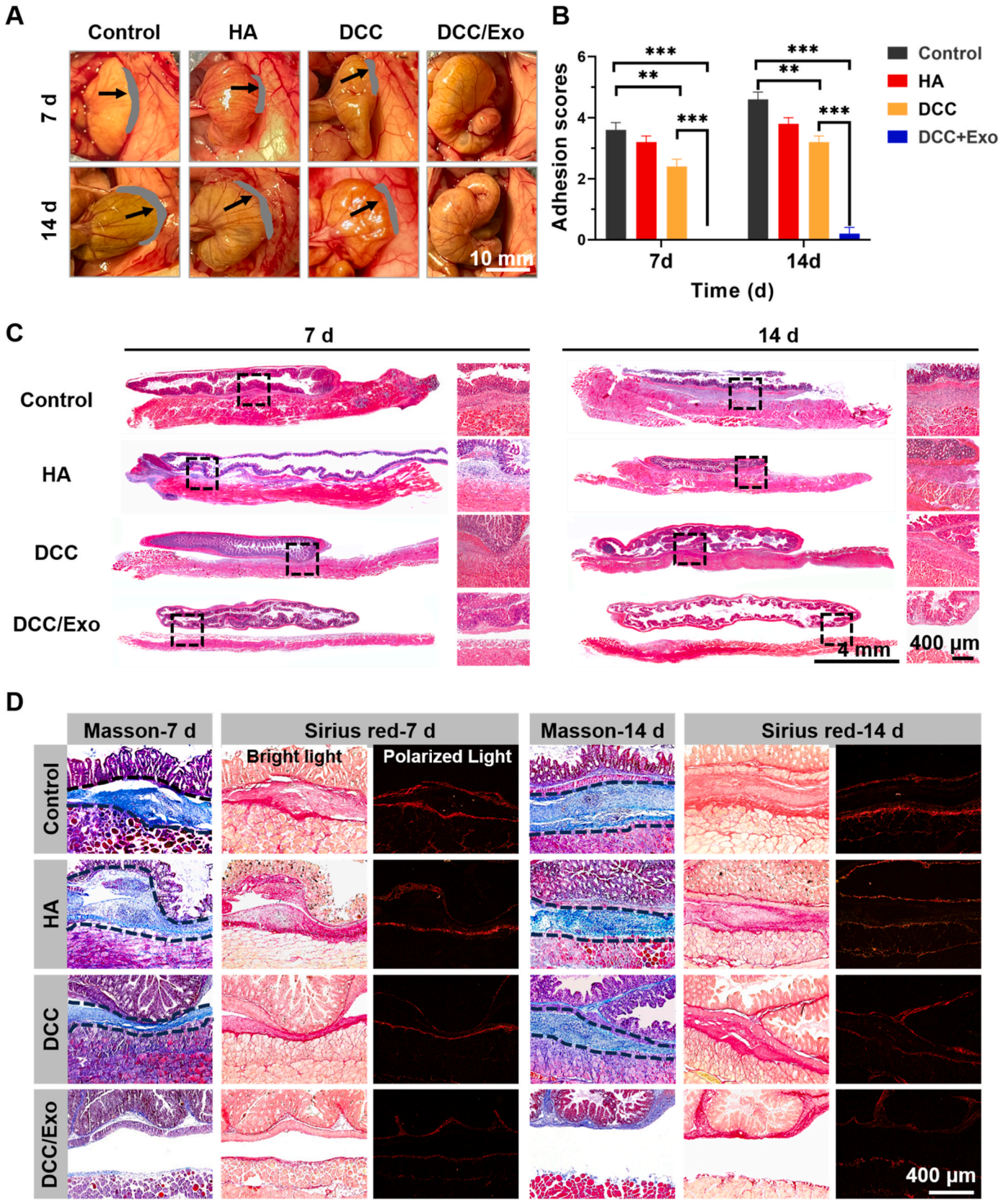

Fig. 7. Anti-adhesion effects of the DCC/Exo. (A) Gross photos of PA. (B) The adhesion scores ($n = 5$, $^{*}p < 0.05$, $^{**}p < 0.01$, $^{***}p < 0.001$). (C) H&E staining images and (D) Masson trichrome staining and Sirius red staining images of the different groups ($n = 3$). (For interpretation of the references to color in this figure legend, the reader is referred to the Web version of this article.)

tissue, and many leukocytes were observed. Moderate adhesions were observed in both the HA and DCC hydrogels, with connections formed between the cecum and the adjacent abdominal wall. Furthermore, although Exos injection alone showed some beneficial effects in preventing adhesions, the thin adhesion can be observed (Fig. S12). This may be due to the anatomical characteristics of the peritoneum, where the injected Exos tend to flow away from the injured site, thus reducing their local retention and efficacy. In contrast, the DCC/Exo group resulted in the absence of adhesions due to the physical barrier function of DCC and the microenvironment modulate function of Exos. Furthermore, the presence of the DCC carrier significantly enhances the retention of Exos at the wound site, thereby creating favorable conditions for their therapeutic function. A renewed mesothelium layer was observed on the injured surfaces of both the cecum and the abdominal wall.

Masson's trichrome and Sirius red staining were used to assess the effects of DCC/Exo on fibrosis levels. As shown in Fig. 7D, on day 7 after surgery, the control group exhibited a significant amount of collagen. Although the commercial HA and DCC hydrogels had some protective effects, there was still noticeable collagen deposition. Consistent with the results of H&E staining, the DCC/Exo group lacked fibrous connective tissue. On day 14 after surgery, the denser fibrous connective tissue in the area connecting the cecum and the abdominal wall in the control group than that on day 7, possibly due to fibrosis caused by continued inflammation. Compared with the HA hydrogel group, the DCC hydrogel had a stronger anti-adhesion ability, but the hydrogels did not play a therapeutic or healing role. Surprisingly, there was almost no collagen deposition in the DCC/Exo group.

Epithelial-mesenchymal transition (EMT) is an essential process in tissue fibrosis [41]. As shown in Fig. S13, a pronounced EMT phenomenon accompanied by the most severe degree of fibrosis was observed in the control group following peritoneal injury. In contrast, both the DCC hydrogel group and the Exo group were able to inhibit the occurrence of EMT. Notably, the DCC/Exo group exhibited significant positive expression of *E*-cadherin and only a limited positive expression of Vimentin, indicating the efficacy of the combined treatment strategy. In summary, the DCC/Exo has satisfactory anti-adhesion effects *in vivo*, and can reduce collagen deposition and promote tissue healing.

4. Discussion

The development of PA involves a series of interconnected events and biological mechanisms, including initial tissue injury, wound healing, fibrinolysis, and fibrosis. Oxidative stress and inflammation are pivotal factors that exert a profound influence on the evolution of PA, driving the complex interplay of cellular and molecular processes that culminate in the formation of adhesions [1]. In this study, the DCC hydrogels were prepared as a physical barrier for the prevention of PA. The preparation of the DCC hydrogel was straightforward, avoiding the use of harmful chemicals and complex reactions, thereby enhancing its potential for clinical use. First, the injection time can be modulated by adjusting the crosslinked degree; the more aldehyde groups present, the shorter gelatin time, which is expected to be a suitable injectable material for clinical use [22]. Second, these hydrogels can be injected quickly via a syringe and cover irregular wounds effectively, further enhancing their effectiveness as a physical barrier against adhesions. Third, the DCC hydrogels demonstrated cytocompatibility and histocompatibility due to the nature of polysaccharide network structure and the green preparation process. Fourth, the appropriate retention time is a key factor for an effective anti-adhesive material. Commercial anti-adhesion hydrogels could reduce adhesions to some extent, but degraded rapidly and had no immunomodulation function. Overall, the prepared DCC hydrogels possess potential advantages in terms of biocompatibility, biodegradability, mechanical properties, and drug delivery. However, they still need to overcome challenges related to stability and clinical acceptability.

The DCC hydrogels served as both a delivery vehicle to enhance Exos retention at designated sites and as a barrier against injury, effectively preventing adhesions. We found that the anti-adhesion effect of the DCC hydrogels was superior to the commercial HA hydrogels, but the DCC hydrogels lacked immunoregulatory properties. Exos play a pivotal role in tissue repair and regeneration owing to their inherent antioxidant and anti-inflammatory properties [42,43]. When the Exos were injected into the peritoneal cavity, they exhibited a tendency to leak, resulting in reduced retention of these Exos in the targeted area. We engineered DCC hydrogel carriers to enhance the localized action of Exos at the injury site, thereby maximizing their therapeutic efficacy. The release kinetics demonstrated that approximately 90 % of Exos gradually released from the DCC hydrogel over a period of 8 days. Furthermore, we injected DCC/Dil-labeled Exos into the subcutis of mice and the results showed that Exos can be taken up by cells, consistent with reports that Exos can be easily perfused into tissues [44–46]. Over time, the red fluorescence in subcutaneous tissue decreased significantly, suggesting that Exos were removed from host cells *in vivo* [37]. Therefore, the DCC hydrogels exhibited effective Exos release during the initial phase of tissue injury.

This study aimed to elucidate the underlying mechanisms of the DCC/Exo system's immunomodulatory effects, offering insights into its potential applications in therapeutic interventions. We identified pathways associated with the downregulated genes through a comparative analysis of the RNA-seq data obtained from both the DCC and DCC/Exo groups with publicly accessible gene expression databases. The related pathways were associated with inflammatory mechanisms, including the PI3K-Akt signaling pathway, cytokine-cytokine receptor interactions, and integrin signaling. It has been reported that activation of the PI3K-Akt pathway leads to a decrease in inflammatory responses [47,48]. The significant reduction in cytokine receptor interactions suggested that the DCC/Exo may regulate the immune microenvironment, potentially prevent the development of adhesions. Furthermore, proper modulation of integrin function is essential in the management of inflammatory responses [49,50]. Consequently, the significant downregulation of DEGs detected by RNA-seq confirmed that DCC/Exo could modulate the immune microenvironment.

Adhesion formation involves multiple pathological processes. Initially, there is a significant damage to mesothelial cells, leading to the accumulation of ROS and subsequently prompting the migration and infiltration of inflammatory cells to the affected area [51]. Then, the process of fibrosis unfolds, involving fibrin deposition and fibroblast proliferation [52]. Oxidative stress generates excess ROS, which are extremely destructive to cells and toxic to mesothelial cells, as well as inducing apoptosis [1,2]. DCC/Exo demonstrated a significant capacity to scavenge excess ROS and protect mitochondria from damage in a mouse model of PA. Furthermore, the introduction of DCC/Exo led to a reduction in apoptosis in the cecum and abdominal wall. In addition, DCC/Exo effectively reduced the levels of proinflammatory cytokines (IL-1β and TNF-α) and diminished the presence of inflammatory cells marked by Ly-6G, CD3, and CD68 in the injured area.

The mouse cecum-abdominal wall adhesion model was used to assess the efficacy of DCC/Exo in prevention of postoperative adhesions *in vivo*. As expected, no adhesions were observed in the DCC/Exo group on days 7 and 14. Furthermore, the dotted hemorrhage in the cecum had resolved and the abdominal wall was almost completely repaired. The adhesion scores (0 on day 7 and 0.2 on day 14) in the DCC/Exo group were the lowest among all experimental groups, indicating the superior efficacy of the DCC/Exo treatment in inhibiting adhesion formation. H&E and Masson's trichrome staining showed a dense accumulation of collagen fibers in the control group, indicating persistent adhesive band formation. Conversely, the abdominal wall and cecum region were completely separated in the DCC/Exo group, with only a limited inflammatory response. Notably, mesothelial cell layer structures were detected in the cecum and peritoneum, indicating a gradual recovery in the injured regions of both the cecum and abdominal wall.

Given the positive results of DCC/Exo treatment, the underlying mechanisms were further investigated. Typically, the immune response

to tissue damage is self-limited, subsiding within a timeframe 1–2 weeks [53]. Immune cell involvement and the duration of immune response significantly influence healing outcomes, impacting both fibrosis and tissue regeneration. Various studies have consistently indicated that the ADSCs-derived Exos play a beneficial role through immunomodulation [54,55]. Early *in vitro* studies have shown that these ADSCs-derived Exos robustly modulate macrophage activity, attenuate inflammatory responses and facilitate the polarization of macrophage towards the anti-inflammatory M2 phenotype. Our animal experiments indicated that the DCC hydrogels provided a beneficial effect in the prevention of PA compared to the control group. However, a higher proportion of M1 macrophages was observed in the cecum and abdominal wall areas. Conversely, DCC/Exo not only considerably promoted tissue healing but also effectively decreased the number of M1 macrophages while increased the number of M2 macrophages. In general, both *in vitro* and *in vivo* studies indicated that DCC/Exo can exert immunomodulatory functions and manage the M1/M2 macrophage phenotype, thereby promoting peritoneal repair effectively.

Although the combined strategy of DCC/Exo has been demonstrated to prevent the formation of PA in mice, this study is still in the basic research stage, and its molecular mechanisms of preventing adhesions and promoting peritoneal regeneration are unclear, making challenges for its application in clinical trials. Furthermore, identifying the specific components of Exos that have anti-adhesion properties will aid in developing targeted therapeutic strategies. Therefore, future research should focus on optimizing hydrogel properties and Exos modification. Developing large-scale production methods for hydrogels and Exos to meet clinical demands is also a key issue that needs to be addressed before clinical translation can be achieved.

5. Conclusion

In conclusion, this study highlighted an innovative therapeutic strategy based on the DCC/Exo system for the prevention of peritoneal adhesions. The DCC hydrogels with injectable, biodegradable and nontoxic properties can be used as safe and effective physical barriers against adhesion formation. Moreover, it can modulate the release behaviors of Exos and augment their retention rate in injured areas. Local delivery of the DCC/Exo *in vivo* reduced oxidative stress and ameliorated inflammation by modulating the relevant immune microenvironment, promoting peritoneal tissue repair and regeneration. Furthermore, the introduction of Exos inhibited the polarization of macrophages toward the M1 phenotype and promoted polarization toward the M2 phenotype. Therefore, the constructed DCC/Exo system prevents the formation of postoperative adhesions effectively. This proposed strategy may also serve as a template for the design of combined therapeutic modality for human diseases.

CRediT authorship contribution statement

Weitong Wang: Writing – original draft, Software, Methodology, Data curation. **Yuchen Ren:** Methodology, Data curation. **Qingyu Yu:** Writing – original draft, Methodology, Conceptualization. **Lijie Jiang:** Methodology, Data curation. **Chaojie Yu:** Methodology, Data curation. **Zhiwei Yue:** Methodology. **Yue Wang:** Data curation. **Jiajun Lu:** Data curation. **Pengcheng Che:** Supervision, Resources, Funding acquisition. **Junjie Li:** Writing – review & editing, Funding acquisition. **Hong Sun:** Writing – review & editing, Supervision, Funding acquisition.

Declaration of competing interest

The authors declare that they have no known competing financial interests or personal relationships that could have appeared to influence the work reported in this paper.

Acknowledgments

This work was financially supported by the Natural Science Foundation of Hebei Province, China (No.H2023209021 & No. H2024209013). Hebei Key Laboratory for Rehabilitation Engineering and Regenerative Medicine (SZX202327). Tangshan Science and Technology Bureau (No.22150201A). The National Natural Science Foundation of China (No. U20A20261). The Fundamental Research Funds for the Central Universities (No.3332023072).

Appendix A. Supplementary data

Supplementary data to this article can be found online at https://doi.org/10.1016/j.mtbio.2024.101312.

Data availability

Data will be made available on request.

References

[1] J. Tang, Z. Xiang, M.T. Bernards, S. Chen, Peritoneal adhesions: occurrence, prevention and experimental models, Acta Biomater. 116 (2020) 84–104.
[2] T. Shen, Y. Wu, X. Wang, Z. Wang, E. Li, C. Zhou, C. Yue, Z. Jiang, G. Wei, J. Lian, Q. Xu, X. Li, Activating SIRT3 in peritoneal mesothelial cells alleviates postsurgical peritoneal adhesion formation by decreasing oxidative stress and inhibiting the NLRP3 inflammasome, Exp. Mol. Med. 54 (9) (2022) 1486–1501.
[3] P. Krielen, M.W.J. Stommel, P. Pargmae, N.D. Bouvy, E.A. Bakkum, H. Ellis, M. C. Parker, E.A. Griffiths, H. van Goor, R.P.G. Ten Broek, Adhesion-related readmissions after open and laparoscopic surgery: a retrospective cohort study (SCAR update), Lancet 395 (10217) (2020) 33–41.
[4] L. Jiang, F. Yao, E. Zhang, Q. Yu, C. Yu, Z. Chen, J. Chen, Z. Yue, P. Che, J. Li, H. Sun, Combined treatment of xyloglucan derivative hydrogel and anti-C5a receptor antibody in preventing peritoneal adhesion, Acta Biomater. 151 (2022) 163–173.
[5] Z. Song, Y. Zhang, H. Shao, Y. Ying, X. Chen, L. Mei, X. Ma, L. Chen, P. Ling, F. Liu, Effect of xanthan gum on the prevention of intra-abdominal adhesion in rats, Int. J. Biol. Macromol. 126 (2019) 531–538.
[6] B. Liu, Y. Kong, O.A. Alimi, M.A. Kuss, H. Tu, W. Hu, A. Rafay, K. Vikas, W. Shi, M. Lerner, W.L. Berry, Y. Li, M.A. Carlson, B. Duan, Multifunctional microgel-based cream hydrogels for postoperative abdominal adhesion prevention, ACS Nano 17 (4) (2023) 3847–3864.
[7] Y.C. Shin, W.J. Yang, J.H. Lee, J.W. Oh, T.W. Kim, J.C. Park, S.H. Hyon, D.W. Han, PLGA nanofiber membranes loaded with epigallocatechin-3-O-gallate are beneficial to prevention of postsurgical adhesions, Int. J. Nanomed. 9 (2014) 4067–4078.
[8] G. Wei, Y. Wu, Q. Gao, C. Zhou, K. Wang, C. Shen, G. Wang, K. Wang, X. Sun, X. Li, Effect of emodin on preventing postoperative intra-abdominal adhesion formation, Oxid. Med. Cell. Longev. 2017 (2017) 1740317.
[9] K. Lv, P. Lou, S. Liu, Y. Wang, J. Yang, P. Zhou, X. Zhou, Y. Lu, H. Wang, J. Cheng, J. Liu, Injectable multifunctional composite hydrogel as a combination therapy for preventing postsurgical adhesion, Small (2023) e2303425.
[10] C. Chang, J. Yan, Z. Yao, C. Zhang, X. Li, H.Q. Mao, Effects of mesenchymal stem cell-derived paracrine signals and their delivery strategies, Adv. Healthcare Mater. 10 (7) (2021) e2001689.
[11] X. Wu, H. Zhu, J. Che, Y. Xu, Q. Tan, Y. Zhao, Stem cell niche-inspired microcarriers with ADSCs encapsulation for diabetic wound treatment, Bioact. Mater. 26 (2023) 159–168.
[12] Y. Dong, M. Cui, J. Qu, X. Wang, S.H. Kwon, J. Barrera, N. Elvassore, G.C. Gurtner, Conformable hyaluronic acid hydrogel delivers adipose-derived stem cells and promotes regeneration of burn injury, Acta Biomater. 108 (2020) 56–66.
[13] P. Li, X. Guo, A review: therapeutic potential of adipose-derived stem cells in cutaneous wound healing and regeneration, Stem Cell Res. Ther. 9 (1) (2018) 302.
[14] N.B. Vu, H.T. Nguyen, R. Palumbo, R. Pellicano, S. Fagoonee, P.V. Pham, Stem cell-derived exosomes for wound healing: current status and promising directions, Minerva Med. 112 (3) (2021) 384–400.
[15] S. Alatab, S. Shekarchian, I. Najafi, R. Moghadasali, N. Ahmadbeigi, M. R. Pourmand, T. Bolurieh, N. Jaroughi, G. Pourmand, N. Aghdami, Systemic infusion of autologous adipose tissue-derived mesenchymal stem cells in peritoneal dialysis patients: feasibility and safety, Cell J 20 (4) (2019) 483–495.
[16] E.C. Costalonga, C. Fanelli, M.R. Garnica, I.L. Noronha, Adipose-derived mesenchymal stem cells modulate fibrosis and inflammation in the peritoneal fibrosis model developed in uremic rats, Stem Cell. Int. 2020 (2020) 3768718.
[17] L. Mazini, L. Rochette, B. Admou, S. Amal, G. Malka, Hopes and limits of adipose-derived stem cells (ADSCs) and mesenchymal stem cells (MSCs) in wound healing, Int. J. Mol. Sci. 21 (4) (2020) 1306.
[18] C.Y. Yang, P.Y. Chang, J.Y. Chen, B.S. Wu, A.H. Yang, O.K. Lee, Adipose-derived mesenchymal stem cells attenuate dialysis-induced peritoneal fibrosis by modulating macrophage polarization via interleukin-6, Stem Cell Res. Ther. 12 (1) (2021) 193.

[19] A. Casado-Díaz, J.M. Quesada-Gómez, G. Dorado, Extracellular vesicles derived from mesenchymal stem cells (MSC) in regenerative medicine: applications in skin wound healing, Front. Bioeng. Biotechnol. 8 (2020) 146.
[20] P. Wu, B. Zhang, H. Shi, H. Qian, W. Xu, MSC-exosome: a novel cell-free therapy for cutaneous regeneration, Cytotherapy 20 (3) (2018) 291–301.
[21] C.R. Harrell, N. Jovicic, V. Djonov, N. Arsenijevic, V. Volarevic, Mesenchymal stem cell-derived exosomes and other extracellular vesicles as new remedies in the therapy of inflammatory diseases, Cells 8 (12) (2019) 1605.
[22] Q. Yu, H. Sun, Z. Yue, C. Yu, L. Jiang, X. Dong, M. Yao, M. Shi, L. Liang, Y. Wan, H. Zhang, F. Yao, J. Li, Zwitterionic polysaccharide-based hydrogel dressing as a stem cell carrier to accelerate burn wound healing, Adv. Healthcare Mater. 12 (7) (2023) e2202309.
[23] J. Hu, I. Altun, Z. Zhang, H. Albadawi, M.A. Salomao, J.L. Mayer, L. Hemachandra, S. Rehman, R. Oklu, Bioactive-tissue-derived nanocomposite hydrogel for permanent arterial embolization and enhanced vascular healing, Adv. Mater. 32 (33) (2020) e2002611.
[24] Q. Yu, Z. Yue, C. Yu, L. Liang, M. Yao, C. Chen, Y. Zhao, L. Jiang, H. Sun, F. Yao, J. Li, Photo-mediated zwitterionic hydrogel as “blocked” platform for expansion and maintaining stemness of stem cells, Appl. Mater. Today 31 (2023) 101773.
[25] H. Ning, H. Chen, J. Deng, C. Xiao, M. Xu, L. Shan, C. Yang, Z. Zhang, Exosomes secreted by FNDC5-BMMSCs protect myocardial infarction by anti-inflammation and macrophage polarization via NF-κB signaling pathway and Nrf2/HO-1 axis, Stem Cell Res. Ther. 12 (1) (2021) 519.
[26] S. Deng, H. Cao, X. Cui, Y. Fan, Q. Wang, X. Zhang, Optimization of exosome-based cell-free strategies to enhance endogenous cell functions in tissue regeneration, Acta Biomater. 171 (2023) 68–84.
[27] E. Zhang, Q. Guo, F. Ji, X. Tian, J. Cui, Y. Song, H. Sun, J. Li, F. Yao, Thermoresponsive polysaccharide-based composite hydrogel with antibacterial and healing-promoting activities for preventing recurrent adhesion after adhesiolysis, Acta Biomater. 74 (2018) 439–453.
[28] L. Li, N. Wang, X. Jin, R. Deng, S. Nie, L. Sun, Q. Wu, Y. Wei, C. Gong, Biodegradable and injectable in situ cross-linking chitosan-hyaluronic acid based hydrogels for postoperative adhesion prevention, Biomaterials 35 (12) (2014) 3903–3917.
[29] M. Wang, S. Lin, M. Liu, J. Jiao, H. Mi, J. Sun, Y. Liu, R. Guo, S. Liu, H. Fu, Y. Yang, R. Li, An injectable and rapidly degraded carboxymethyl chitosan/polyethylene glycol hydrogel for postoperative antiadhesion, Chem. Eng. J. 463 (2023) 142283.
[30] J. Zhao, X. Li, J. Hu, F. Chen, S. Qiao, X. Sun, L. Gao, J. Xie, B. Xu, Mesenchymal stromal cell-derived exosomes attenuate myocardial ischaemia-reperfusion injury through miR-182-regulated macrophage polarization, Cardiovasc. Res. 115 (7) (2019) 1205–1216.
[31] Q. Hu, X. Xia, X. Kang, P. Song, Z. Liu, M. Wang, W. Guan, S. Liu, A review of physiological and cellular mechanisms underlying fibrotic postoperative adhesion, Int. J. Biol. Sci. 17 (1) (2021) 298–306.
[32] M.P. Diamond, Reduction of postoperative adhesion development, Fertil. Steril. 106 (5) (2016) 994–997.e991.
[33] N. Uyama, H. Tsutsui, S. Wu, K. Yasuda, E. Hatano, X.Y. Qin, S. Kojima, J. Fujimoto, Anti-interleukin-6 receptor antibody treatment ameliorates postoperative adhesion formation, Sci. Rep. 9 (1) (2019) 17558.
[34] J. Yeo, J. Lee, S. Yoon, W.J. Kim, Tannic acid-based nanogel as an efficient anti-inflammatory agent, Biomater. Sci. 8 (4) (2020) 1148–1159.
[35] A. Awadasseid, Y. Wu, W. Zhang, Extracellular vesicles (Exosomes) as immunosuppressive mediating variables in tumor and chronic inflammatory microenvironments, Cells 10 (10) (2021) 2533.
[36] B. Mi, Y. Xiong, L. Lu, J. Liao, G. Liu, Y. Zhao, Macrophage-mediated fracture healing: unraveling molecular mechanisms and therapeutic implications using hydrogel-based interventions, Biomaterials 305 (2024) 122461.
[37] L. Xin, X. Lin, F. Zhou, C. Li, X. Wang, H. Yu, Y. Pan, H. Fei, L. Ma, S. Zhang, A scaffold laden with mesenchymal stem cell-derived exosomes for promoting endometrium regeneration and fertility restoration through macrophage immunomodulation, Acta Biomater. 113 (2020) 252–266.
[38] D. Yang, L. Yang, J. Cai, X. Hu, H. Li, X. Zhang, X. Zhang, X. Chen, H. Dong, H. Nie, Y. Li, A sweet spot for macrophages: focusing on polarization, Pharmacol. Res. 167 (2021) 105576.
[39] I. Lua, Y. Li, L.S. Pappoe, K. Asahina, Myofibroblastic conversion and regeneration of mesothelial cells in peritoneal and liver fibrosis, Am. J. Pathol. 185 (12) (2015) 3258–3273.
[40] R.P. ten Broek, Y. Issa, E.J. van Santbrink, N.D. Bouvy, R.F. Kruitwagen, J. Jeekel, E.A. Bakkum, M.M. Rovers, H. van Goor, Burden of adhesions in abdominal and pelvic surgery: systematic review and met-analysis, Bmj 347 (2013) f5588.
[41] Q. Peng, W. Wu, K.Y. Wu, B. Cao, C. Qiang, K. Li, S.H. Sacks, W. Zhou, The C5a/C5aR1 axis promotes progression of renal tubulointerstitial fibrosis in a mouse model of renal ischemia/reperfusion injury, Kidney Int. 96 (1) (2019) 117–128.
[42] C. Xia, Z. Dai, Y. Jin, P. Chen, Emerging antioxidant paradigm of mesenchymal stem cell-derived exosome therapy, Front. Endocrinol. 12 (2021) 727272.
[43] W. Zhang, R. Liu, Y. Chen, M. Wang, J. Du, Crosstalk between oxidative stress and exosomes, Oxid. Med. Cell. Longev. 2022 (2022) 3553617.
[44] F. Malekian, A. Shamsian, S.P. Kodam, M. Ullah, Exosome engineering for efficient and targeted drug delivery: current status and future perspective, J. Physiol. 601 (22) (2023) 4853–4872.
[45] P.A. Shiekh, A. Singh, A. Kumar, Exosome laden oxygen releasing antioxidant and antibacterial cryogel wound dressing OxOBand alleviate diabetic and infectious wound healing, Biomaterials 249 (2020) 120020.
[46] J. Wang, D. Chen, E.A. Ho, Challenges in the development and establishment of exosome-based drug delivery systems, J. Contr. Release 329 (2021) 894–906.
[47] S. Shen, T. Sun, X. Ding, X. Gu, Y. Wang, X. Ma, Z. Li, H. Gao, S. Ge, Q. Feng, The exoprotein Gbp of Fusobacterium nucleatum promotes THP-1 cell lipid deposition by binding to CypA and activating PI3K-AKT/MAPK/NF-κB pathways, J. Adv. Res. (2024) 93–105.
[48] M. Shi, H. Liu, T. Zhang, M. Zhang, X. Tang, Z. Zhang, W. Lu, S. Yang, Z. Jiang, Q. Cui, Z. Li, Extracellular vesicles derived from adipose mesenchymal stem cells promote peritoneal healing by activating MAPK-ERK1/2 and PI3K-Akt to alleviate postoperative abdominal adhesion, Stem Cell. Int. 2022 (2022) 1940761.
[49] M.E. Keir, F. Fuh, R. Ichikawa, M. Acres, J.A. Hackney, G. Hulme, C.D. Carey, J. Palmer, C.J. Jones, A.K. Long, J. Jiang, S. Klabunde, J.C. Mansfield, C. M. Looney, W.A. Faubion, A. Filby, J.A. Kirby, J. McBride, C.A. Lamb, Regulation and role of αE integrin and gut homing integrins in migration and retention of intestinal lymphocytes during inflammatory bowel disease, J. Immunol. 207 (9) (2021) 2245–2254.
[50] S. Pulikkot, L. Hu, Y. Chen, H. Sun, Z. Fan, Integrin regulators in neutrophils, Cells 11 (13) (2022) 2025.
[51] J. Chen, X. Tang, Z. Wang, A. Perez, B. Yao, K. Huang, Y. Zhang, M.W. King, Techniques for navigating postsurgical adhesions: insights into mechanisms and future directions, Bioeng Transl Med 8 (6) (2023) e10565.
[52] A. Fatehi Hassanabad, A.N. Zarzycki, K. Jeon, J.F. Deniset, P.W.M. Fedak, Post-operative adhesions: a comprehensive review of mechanisms, Biomedicines 9 (8) (2021) 867.
[53] J. Zarubova, M.M. Hasani-Sadrabadi, R. Ardehali, S. Li, Immunoengineering strategies to enhance vascularization and tissue regeneration, Adv. Drug Deliv. Rev. 184 (2022) 114233.
[54] T. Wang, Z. Jian, A. Baskys, J. Yang, J. Li, H. Guo, Y. Hei, P. Xian, Z. He, Z. Li, N. Li, Q. Long, MSC-derived exosomes protect against oxidative stress-induced skin injury via adaptive regulation of the NRF2 defense system, Biomaterials 257 (2020) 120264.
[55] D. Zhu, T.K. Johnson, Y. Wang, M. Thomas, K. Huynh, Q. Yang, V.C. Bond, Y. E. Chen, D. Liu, Macrophage M2 polarization induced by exosomes from adipose-derived stem cells contributes to the exosomal proangiogenic effect on mouse ischemic hindlimb, Stem Cell Res. Ther. 11 (1) (2020) 162.